J Mater Sci (2007) 42:7729–7737
DOI 10.1007/s10853-007-1658-y

Numerical simulation of rapid solidification of a spherical sample on a metallic substrate

Zoran S. Nikolic · Masahiro Yoshimura

Received: 13 September 2006 / Accepted: 5 March 2007 / Published online: 3 June 2007

Abstract Since the exact analytical solutions for rapid solidification process are available only for special boundary conditions, numerical techniques have to be applied for more general boundary conditions. In this paper we will describe a finite difference method for simulation of rapid solidification that is based on control volume methodology and interface-tracking technique. Heat transfer computer study will be realized for solidification with and without melt undercooling at the interface. Such numerical method will be applied for thermal history analysis of solidifying nickel on copper substrate.

Introduction

Rapid quenching of the melt has attracted much attention because of the large potential for new material properties originating in the refinement of the cast structure, extended solid solubility, metastable crystalline phases and amorphous alloys [1]. To get rapidly quenched samples of high temperature materials, many techniques have been developed. Some of them, such as splat cooling, melt-spinning, spray deposition and strip casting are based on bringing the melt in intimate contact with a substrate. However, rapid solidification is not easily accessible experimentally due to the simultaneously small time and spatial scales. Especially because of the high cooling rates realized it is difficult to measure the relevant process parameters. Therefore attempts have been made to calculate the operating conditions for the formation of crystalline and amorphous alloys from heat flow models. Even more, numerical investigation of these processes becomes very important for the understanding of the underlying physics together with information, such as local temperature distribution, solid–liquid interface velocity etc.

Generally speaking, complex solidification kinetics can be solved only by using numerical techniques. Numerical methods for simulation of solidification processes can be categorized as fixed-grid or interface tracking schemes. Unfortunately, former one cannot accurately track a sharp solid–liquid interface. Tracking the interface location accurately can be provided by modification of fix-grid schemes, such as, for example, the node-jumping scheme [2] or the element subdivision method [3]. Interface-tracking techniques can be used for solidification without undercooling [4, 5] as well as for solidification with undercooling [6].

Recently Nikolic et al. [7] adopted numerical model to analyze heat transfer process during solidification of sample melted in Arc-image furnace [8, 9], where the melt cooling rate and the solidification rate are controlled by the interfacial heat transfer conditions between spherical sample and colder substrate. The governing heat conduction equations for solidifying sample and substrate as a heat sink were derived assuming spherical symmetry. It should be noted, however, that both contact resistance and undercooling are also very important issues in modeling this type of solidification, especially under non-equilibrium

Z. S. Nikolic (✉)
Faculty of Electronic Engineering,
Department of Microelectronics, University of Nish,
Nish PO Box 73, 18000, Serbia
e-mail: znikolic@elfak.ni.ac.yu

M. Yoshimura
Materials and Structure Laboratory, Center for Materials Design,
Tokyo Institute of Technology, Yokohama 226-8503, Japan

conditions where large undercooling may exist. Therefore, in this paper we will describe a finite difference method based on control volume methodology and interface-tracking technique for simulation of solidification with and without undercooling. Such numerical method can be use for thermal history analysis in both sample and substrate, including the phase change phenomena. Also, the effects of process parameters on solidification of sample on substrate can be investigate numerically. The parameters include sample size, contact area size between the sample and substrate and degree of undercooling associated with rapid phase change and moving interface.

Mathematical modeling

Problem description

We will define two-dimensional (2-D) heat transfer model by considering solidification of the solid spherical sample placed on the solid substrate of a finite size and cooled by water. Numerical method that will be defined will simulate the solidification process on whole. This radially symmetric heat-conduction model problem can be solved numerically if we assume a non-uniform temperature distribution inside the sample, and symmetric about the growth axis (which coincides with direction substrate–sample), because the solidification starts at some discrete points on the contact surface between substrate (heat sink) and sample. It means that this problem becomes 2-D (multi-dimensional effects are believed to be small for cooling and solidification processes).

The governing heat conduction equations for solidifying sample on the substrate, assuming constant conductivity, can be written as

$$\frac{\partial^2 T_p}{\partial x^2} + \frac{\partial^2 T_p}{\partial y^2} = \frac{\rho_p c_p}{\lambda_p}\frac{\partial T_p}{\partial t} \tag{1}$$

where T is temperature, ρ is the density, c is the specific heat capacity, λ is the thermal conductivity, t is time, and the subscript $p = 1$, 2 or 3 represents melt, solid and substrate, respectively. For numerical solution of these equations we will assume that the rectangular experimental region is replaced by finite difference mesh containing a finite number of grid points where the mesh is defined by grid spacings Δx and Δy for Cartesian coordinates x and y, respectively. In this 2-D computational space we will put sample and substrate as separated and by interface connected domains. Using control-volume (CV) definition [8], the domain will be a region that is equitably divided into n interconected boundary and internal CVs halfway between neighboring grid (node) points (x_k ,y_k), i.e.

$$D = \{\ \mathrm{CV}^k\} = \{\mathrm{CV}(x_k, y_k)\}\ \ (k = 1, 2, \ldots, n).$$

If the mesh spacing is constant ($\Delta x = \Delta y$) the internal grid points will be at the center of the CVs.

The entire solidification process will be divided into three stages: (i) melt (liquid) cooling, (ii) melt solidifying, and finally (iii) solidified sample cooling. For each stage corresponding numerical model will be defined. At the beginning of the solidification process, the spherical sample is assumed to be at a uniform temperature T_o, the water-cooled substrate at uniform temperature T_{sub}, and the surrounding medium (air) at temperature T_{amb} (ambient temperature). The latter two temperatures are well-bellow the equilibrium melting temperature of the sample (T_m).

Melt cooling

Since there are no heat sources inside the sample, the sample surface temperature starts to decrease due to the heat transfer from the sample to the colder substrate and to the ambient. The thermal contact between the sample and the substrate is quantified by an interfacial heat transfer coefficient defined as

$$h = \frac{q(t)}{\langle T_{\mathrm{sam}}\rangle - \langle T_{\mathrm{sub}}\rangle},$$

where $q(t)$ is the time-dependent heat flux through the interface from the sample to the substrate, and $\langle T_{\mathrm{sam}}\rangle$ and $\langle T_{\mathrm{sub}}\rangle$ are the average temperatures of the sample and the substrate at the contact interface, respectively. If the coefficient h is known, then the temperature at the interface can be computed by equations

$$-\lambda_p \left.\frac{\partial T_p(x,y)}{\partial y}\right|_I = h \cdot (\langle T_{\mathrm{sam}}\rangle - \langle T_{\mathrm{sub}}\rangle),$$

where the subscript p = 1,2,3 has the same meanings as in Eq. 1.

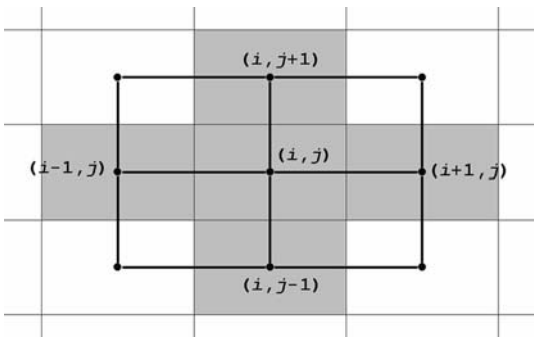

Fig. 1 Interior control volume with its four first neighbors and corresponding grid points

For an approximate solution of the Eq. 1 on interior grid points (Fig. 1) of the sample and the substrate, the explicit method [9] will be used. Since the boundary CVs of the sample can be exposed to some convection boundary condition, the temperature at the sample surface must be computed differently than on interior CVs. In that sense, several CV configurations should be considered and for each of them corresponding nodal energy balance equation with stability criterion will be used [9]. In these equations Biot number defined in the finite-difference form as

$$Bi = \frac{h_c \Delta x}{\lambda}$$

provides a measure of the internal conduction resistance relative to the external heat transfer resistance, where h_c is the convective heat transfer coefficient. If the sample surface is adiabatic, the energy balance equations and corresponding stability criterions should be modified by setting Bi equal to zero. In our approach we will also include an effective Biot number defined by using the combined heat transfer coefficient as a sum of the convective and the radiative heat transfer coefficients, i.e.

$$h_c + h_r = h_c + \varepsilon\sigma \frac{T^4(x,y) - T_{\text{amb}}^4}{T(x,y) - T_{\text{amb}}}, \tag{2}$$

where ε is the total hemispherical emissivity and σ is Stefan–Bolzmann constant.

Since the sample is much smaller than the water-cooled substrate, boundary condition for rectangular substrate far away from the interface sample–substrate is assumed to be constant (T_{sub}).

Nucleation and solidification

Let we assume that the interface substrate–sample is stable through the entire solidification process. We further assume that solidification starts at time t_1 on the sample surface across the contact interface with the substrate at the nucleation temperature T_n. During this process interface starts to change from an initial liquid–solid contact (interfacial area defined by CVs on the interface) to a solid–solid contact. After that the liquid–solid interface position, which follows the axisymmetric geometry for this model experiment (Fig. 2), will be defined by the local equilibrium condition at the solid–liquid interface

$$\rho_s v_I L = \lambda_s \left.\frac{\partial T_s}{\partial y}\right|_I - \lambda_\ell \left.\frac{\partial T_\ell}{\partial y}\right|_I \tag{3}$$

where T_ℓ and T_s are the temperatures of the melt and solid phase, respectively, L is the latent heat of solidification, and

$$v_I = \frac{\mathrm{d}w}{\mathrm{d}t} \tag{4}$$

is the velocity of the solid–liquid interface, where w is the thickness of the solidified layer.

Introduction of CVs will allow us to track interface across the neighboring CVs in horizontal and vertical directions inside the sample with increased interface tracking resolution. Let $\mathrm{CV}(x_k, y_k) \equiv \mathrm{CV}_{i,j}$ is the central control volume and $\mathrm{CV}_{i\text{-}1,j}$, $\mathrm{CV}_{i+1,j}$, $\mathrm{CV}_{i,j\text{-}1}$ and $\mathrm{CV}_{i,j+1}$ are its first neighbors, as depicted in Fig. 1. During solidification these CVs can be partially or fully liquid or solid. If two adjoined CVs are of different states then the interface solid–liquid in between them exist. Our analysis showed that according to the states of neighboring CVs and the position of interface between them within elemental cell (Fig. 1) several different configurations exist, where the typical one is sketched in Fig. 3. For computation of time-dependent temperature, $T(x,y,t)$, we will now use implicit finite difference equations [9], which will be solved using Gaussian elimination algorithm. Our numerical method will be adopted to track the location of the curved interface solid-liquid between CVs of different state as well as across CVs that represent solid or liquid phase. Such approach will be able to calculate accurately the interface parameters, such as interface velocity and interface temperature. Heat transfer study will be realized as solidification without undercooling and as solidification characterized by melt undercooling at the interface. Mathematical model for interface tracking with and without undercooling will be similar to approach of Wang and Matthys [3] but adopted for spherical sample–substrate solidification model and extended for 2-D case.

Solidification without undercooling

We will assume that solidification with no undercooling begins on the bottom sample surface across the contact interface with the colder substrate when the sample surface temperature reaches the equilibrium melting temperature (local equilibrium condition at the solid–liquid interface, i.e., $T(x,y) = T_m$). Since the solidification rate is determined by the rate of heat removal at the interface, the consecutive positions of the interface solid–liquid (Fig. 2) will be directly computed by solving Eq. 3 in both horizontal and vertical directions.

If the interface solid–liquid is 2-D in nature and has a symmetry axis going from the bottom sample (nucleation region) to the top of the sample or from the sample surface toward its interior, then the discrete value of the interface velocity (4) can be replaced by

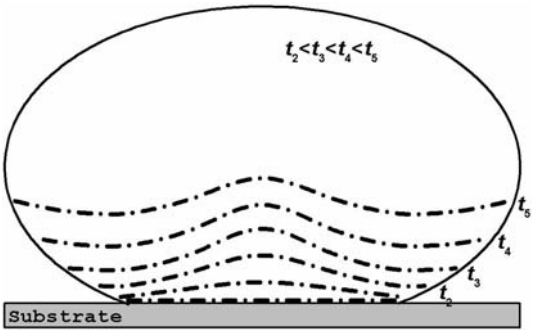

Fig. 2 Sketch of solid–liquid interface positions during solidification

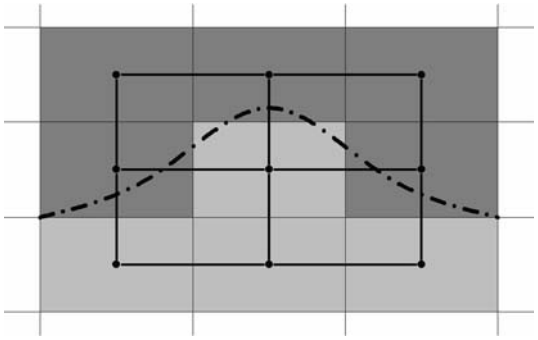

Fig. 3 Possible interface shape and location and the configuration of solid and liquid CVs during solidification. Liquid CVs are dark and solid CVs are gray features. Interface is drawn by black dashed line

$$v_{I(k)} = \frac{w_k^{n+1} - w_k^n}{\Delta t},$$

where the superscripts n and $n + 1$ indicate the positions of the interface for previous and current time steps, and the subscript k stands for either horizontal (i) or vertical (j) directions. Fixing the interface temperature to the melting temperature, and if $T_{i,j\text{-}1}^{s,n}$ and $T_{i,j}^{\ell,n}$ are the temperatures of solidified $CV_{i,j\text{-}1}$ and liquid $CV_{i,j}$ at previous time step, then the new interface position between them can be computed by the equation

$$w_j^{n+1} = w_j^n + \frac{\Delta t}{\rho_s L}\left[\lambda_s \frac{T_m - T_{i,j-1}^{s,n}}{a\Delta x} - \lambda_\ell \frac{T_{i,j}^{\ell,n} - T_m}{b\Delta x}\right], \qquad (5)$$

where $a\Delta x$ and $b\Delta x$ are the distances between the interface position (w_j^n) and the centers of $CV_{i,j\text{-}1}$ and $CV_{i,j}$, respectively. Equation 5 produces uniform solid–liquid interface displacement. The only problem can be the temperature gradient in front of the interface during early stage of solidification. It can dominate and then has destabilizing influence on the interface computation. Similar equations will be written for the interface between solidified $CV_{i\text{-}1,j}$ and liquid $CV_{i,j}$

$$w_i^{n+1} = w_i^n + \frac{\Delta t}{\rho_s L}\left[\lambda_s \frac{T_m - T_{i-1,j}^{s,n}}{c\Delta x} - \lambda_\ell \frac{T_{i,j}^{\ell,n} - T_m}{d\Delta x}\right],$$

as well as between solidified $CV_{i+1,j}$ and liquid $CV_{i,j}$

$$w_i^{n+1} = w_i^n + \frac{\Delta t}{\rho_s L}\left[\lambda_s \frac{T_m - T_{i+1,j}^{s,n}}{c\Delta x} - \lambda_\ell \frac{T_{i,j}^{\ell,n} - T_m}{d\Delta x}\right],$$

where $c\Delta x$ and $d\Delta x$ are the distances between the interface position (w_i^n) and the centers of corresponding solidified and liquid CVs.

Solidification with undercooling

When the undercooling is introduced as a variable, it is convenient to assume that the interface recalesces to the equilibrium melting point immediately after nucleation [10]. For this type of solidification, however, we will introduce physical model by focusing on the relationship between the interface velocity (the interface undercooling) and relevant process variables. Since the interface solid–liquid positions are dictated by the undercooling, for small to moderate undercooling the interface velocity can be related to the interface undercooling $\Delta T_k = T_m - T_{I(k)}$ by the linear kinetics relationship [10]

$$v_{I(k)} = \mu_m \Delta T_k, \qquad (6)$$

where μ_m is the linear kinetic coefficient and $T_{I(k)}$ is the interface temperature in direction k. If $T_{I(k)}^n$ is the interface temperature at previous time step, then the new interface position will be determined by the interface velocity $v_{I(k)}^n = v_{I(k)}(T_{I(k)}^n)$ from the equation

$$w_k^{n+1} = w_k^n + v_{I(k)}^n \Delta t. \qquad (7)$$

New temperature distribution in the sample including new interface temperatures will be now computed by solving the full system consisting of implicit schemes for numerical solution of Eq. 1 [9] and the implicit schemes for the interface nodes

$$\left[\frac{\lambda_s}{a\Delta x} + \frac{\lambda_\ell}{b\Delta x}\right] T_{I(j)}^{n+1} - \frac{\lambda_s}{a\Delta x} T_{i,j-1}^{s,n+1} - \frac{\lambda_\ell}{b\Delta x} T_{i,j}^{\ell,n+1} = \rho_s v_{I(j)}^n L,$$

where the distances $a\Delta x$ and $b\Delta x$ will be determined by the Eq. 7. Similar equations will be written for the interface between solidified $CV_{i\text{-}1,j}$ and liquid $CV_{i,j}$ as well as between solidified $CV_{i+1,j}$ and liquid $CV_{i,j}$.

At time t_2 all CVs in the sample will be solidified and next solidification stage starts.

Solidified sample cooling

The time-dependent temperature distribution inside the solidified sample will be computed on the same way as during melt cooling taking corresponding simulation parameters for solid phase.

Results and discussion

The numerical model described above will be applied for the theoretical study of the solidification of nickel spherical sample placed on metallic water-cooled copper substrate. In our study we will illustrate simulation of both types of solidification with and without undercooling. However, it should be noted that the mathematical formulation and the solution methodology developed are general and can be applied for any type of sample materials. In that sense, in our forthcoming paper [11] we will investigate solidification of alumina experimentally and numerically.

The model-experiment will be nickel sample of the diameter 0.003 m placed onto Cu substrate of the diameter 0.05 m, and assumed substrate–sample circular contact surface of the diameter 0.001 m during solidification. For the initial temperature of the sample we will assume melt to be superheated uniformly by 1858 K (T_m + 132 K), and for the substrate and the ambient uniform room temperatures, T_{sub} = 300 K and T_{amb} = 300 K, respectively. The values of thermophysical properties used in simulation are given in Table 1, where the properties are assumed to be independent of solidification temperature, but different for the liquid and solid phases. The interfacial heat transfer coefficient will be assumed to be constant. Although the initial solid–solid point contact between the sample and the substrate will be replaced by solid–liquid surface contact during heating and by solid–solid surface contact during solidification, shrinkage during solidification, as well as separation between sample and substrate due to shrinkage will be neglected. The mesh grid used will be 50 × 50 nodes in both the sample and the substrate.

Table 1 Physical properties of Ni and Cu used for present calculations

	Ni	Cu
T_m (K)	1726	
L (J/kg)	2.9×10^5	
c_ℓ (J/kg K)	620	
c_s (J/kg K)	595	389
λ_ℓ (W/m K)	43	
λ_s (W/m K)	80	394
ρ_ℓ (kg/m^3)	7900	
ρ_s (kg/m^3)	8450	8900
h_c (W/m^2 K)	5×10^3	

As it was mentioned above our approach is based on explicit and implicit finite difference schemes for different solidification regimes. Since the explicit schemes impose restriction on time interval, it will be define as the minimal value of all time intervals obtained by the stability criterions [9]. The same time interval will be used for the implicit schemes, because they do not impose any time interval restriction (unconditionally stable).

The thermal history of nickel will be now determined by the time-dependent balance between the released latent heat and the heat removed from the sample by conduction, convection and radiation. Later one will be consider by using the effective heat transfer coefficient defined by (2). We will consider separately solidification without undercooling and solidification with undercooling.

Solidification without undercooling

After heating (in an Arc-image furnace) nickel sample starts to cool down due to the external heat extraction and internal heat conduction combined with solidification. When the sample bottom surface reaches the equilibrium melting temperature solidification starts immediately and the interface (solidification front) changes from an initial liquid–solid to a solid–solid contact.

The thermal history shown in Fig. 4 reflects the competition between the external heat extraction and internal heat conduction during early solidification period. Although the solidification already started the average sample temperature and the temperature at the sample top are still above T_m; former one due to the temperature in the sample middle which is at that time still close to T_o, and latter one due to slow heat extraction ($h_c = 5 \times 10^3$ W/m^2 K). Because of the large temperature difference between the sample and the substrate and the large interfacial heat transfer coefficient ($h = 1 \times 10^4$ W/m^2 K), the rate of heat conduction dominates the rate of solidification. The interface solid–liquid with fixed interface temperature (T_m) moves into the superheated melt and the heat is conducted away through the solidified sample and the substrate.

Due to the heat conduction just prior to nucleation the substrate interface temperature increases up to the some plateau temperature ~315 K (Fig. 4), which forms a temperature jump at the contact surface (Fig. 5a). This rapid increase of the substrate interface temperature is a consequence of the large and fast heat transfer (high heat flux over a short time) in direction sample–substrate, finite thermal diffusion in substrate (not enough time for heat energy to diffuse into the substrate), but also very good contact between the nickel melt and the substrate. At t_1 = 9.2 ms the solidification starts and temperature gradients

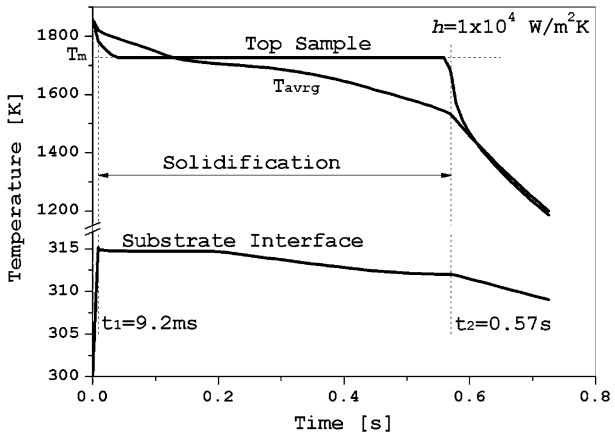

Fig. 4 Time-dependent temperature profiles for the sample (top surface temperature and the average temperature, T_{avrg}) and the substrate interface surface during solidification of nickel on copper substrate (without undercooling)

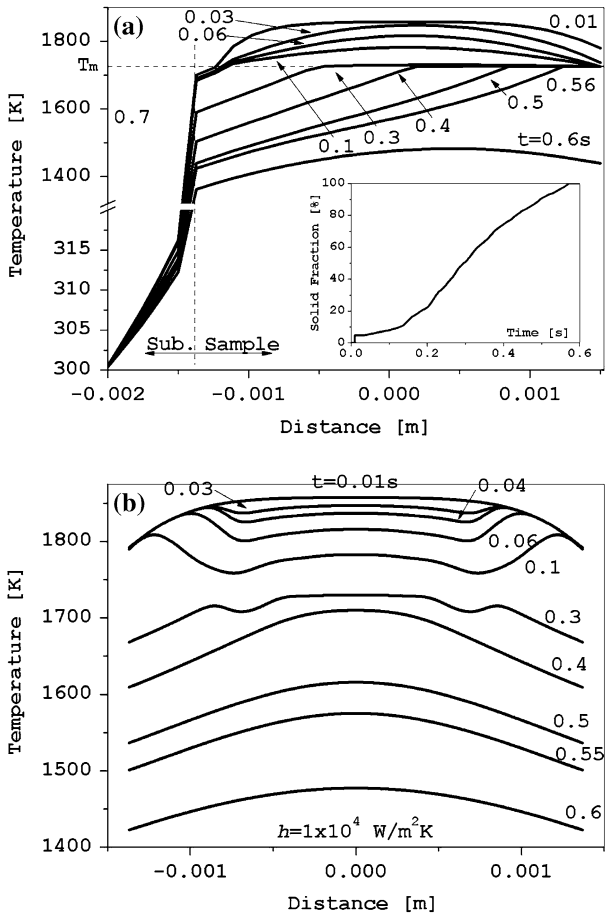

Fig. 5 Temperature evolution across the sample center during solidification of nickel on copper substrate (without undercooling) in (**a**) vertical (substrate–sample) and (**b**) horizontal directions. The inset gives corresponding time-dependent solid fraction

on both sides across the contact surface decrease significantly as the interface liquid–solid moves far away from the sample bottom increasing solid fraction of the sample. It can be seen (Fig. 5) that at the beginning the solidification rate (change in fraction of solid with time) is low but after ~150 ms it approaches almost constant and much higher value (~ 215 %/s from the inset in Fig. 5a). The substrate interface temperature starts to decrease too. The temperature gradient in the liquid part of the sample decreases as the process continues (Fig. 5a). For the late stage of solidification temperature jump approaches uniform value. When the solidification process ended (t_2 = 0.57 s) the sample starts to cool down only.

Figure 5b shows the time-dependent temperature profiles for the middle of the sample in horizontal direction across the center of the sample. It can be seen that main solidification process occurs along growth axis (substrate–sample) mostly due to the heat transfer through the interface sample–substrate, but followed by the solidification on both left and right side along the sample surface. Just after nucleation (0.01 s) the temperature in the center of the sample is close to T_o, whereas on both left and right sides much lower due to the heat extraction through the sample surface. During further solidification temperature along the central line decreases but all CVs are still liquid. At 0.1 s initial convex interface starts to change to concave profile due to formation of solidified layers (solid ''shell'' in three dimensions) on the sample surface boundary. After that solidification progresses by simultaneously solidification of the central part of the sample as well as of solidified layers, which increase in thickness and in height. At 0.3 s the solidification front is already above the sample middle and the solidified layers very close to the sample top. Concave solidification front located now close to *y*-axis goes up and at 0.55 s only the sample top is still liquid. The cooling rate of the sample center during solidification can be estimated to be on the order 0.5×10^3 K/s. Then solidification ends and solidified sample cools down at approximately the same rate everywhere.

Figure 6 shows the influence of the interfacial heat transfer coefficient to the solidification process. Since h defines the rate of heat transfer from the sample to the substrate, it is expected that the shortest solidification time (0.36 s) will be obtained for $h = 5 \times 10^4$ W/m^2 K, compared to 0.41 s obtained for $h = 3 \times 10^4$ W/m^2 K. It can be seen that higher heat transfer from the sample to the substrate increases the substrate interface temperature even to over 360 K in very short time prior to nucleation. However, as the bottom sample nucleates and solidifies, the substrate surface temperature starts to decrease with higher rate corresponding to higher heat transfer coefficient.

Solidification with undercooling

Rapid solidification process is usually accompanied by a large undercooling prior to nucleation at the contact interface substrate–sample, which basically changes solidification kinetic conditions, as it was mentioned above. In our approach the solidification starts when the sample bottom surface reaches the nucleation temperature $T_m - \Delta T$ due to the heat conduction and the interface changes from an initial liquid–solid to a solid–solid contact. The solidification front moves into a supercooled melt, where the melt itself absorbs most of the latent heat and the recalescence takes place. The velocity of moving interface solid–liquid becomes now directly proportional to the undercooling by the linear relationship (6). If the kinetic coefficient μ_m is considerably large one can expect large interface velocity at least in the early stage of the recalescence. However, if this velocity is extremely large the interface can become (numerically) unstable (the negative average gradient due to dominated negative gradient in front of the interface), when some temperature restriction on the solid side must be introduced. During later stage of recalescence melt undercooling is exhausted and this stability problem does not exist any more. In our simulation it will be assumed that $\mu_m = 0.02$ m/s K.

Figure 7 shows the thermal history for solidification of nickel with the undercooling $\Delta T = 100$ K. It is seen that the solidification is delayed because a longer time is needed to cool down melt to the nucleation temperature. When the sample bottom surface temperature drops down just bellow the nucleation temperature (1626 K), the sample top surface cools down bellow the melting temperature due to the heat convection and the radiation, which local minimum depends on the heat transfer coefficient h_c. For $h_c = 5 \times 10^3$ W/m^2 K this minimum is above the nucleation temperature because the heat extraction through the contact surface dominates before nucleation. At the same time, the average temperature of the sample is above T_m due to large superheating that still exist inside the sample. After that nucleation occurs ($t_1 = 33$ ms) and the interface recalesces close to the equilibrium melting temperature depending on the interface velocity (6) and the undercooling. This process is followed by the liberation of great amount of latent heat, which will heat up the liquid sample in front of the interface solid–liquid. It also means that the interface starts to move with high velocity inside the liquid sample, which then produces high solidification rate (up to more than 20% solid fraction in very short time, Fig. 8). Since this released latent heat cannot be transferred through the substrate immediately, the substrate interface temperature reaches its maximum. At this stage the temperature at the interface solid–liquid is already very close to the melting temperature. Therefore the interface velocity starts to decrease and solidification rate decreases too (~530 %/s using the inset in Fig. 8a). The heat transfer through the substrate can continue and the substrate interface temperature decreases. When the solidification ends ($t_1 = 0.183$ s) the solidified sample starts to cool down.

Figure 8 shows the temperature profiles in vertical and horizontal directions across the center of the sample during solidification. The main solidification process occurs in growth axis direction substrate–sample due to the heat transfer through the contact interface sample–substrate. At 0.02 s the melt cools down continuously, whereas the interface is still at temperature above the nucleation temperature, the lateral surfaces above the melting temperature and the middle of the sample just bellow the initial temperature, T_o. At 0.05 s solidification, which started at

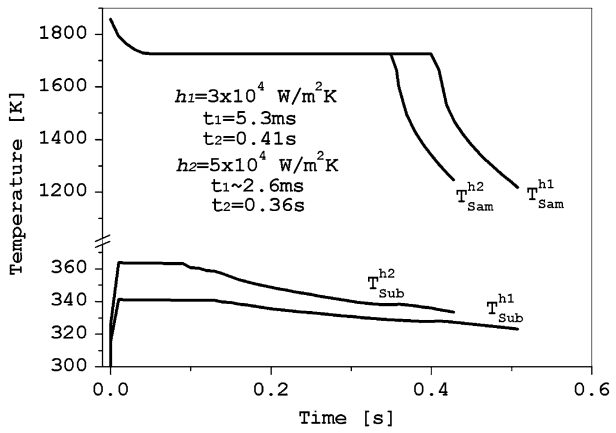

Fig. 6 Dependence of the sample top surface temperature (T_{Sam}) and the substrate interface surface temperature (T_{Sub}) on the interfacial heat transfer coefficient during solidification of nickel on copper substrate (without undercooling)

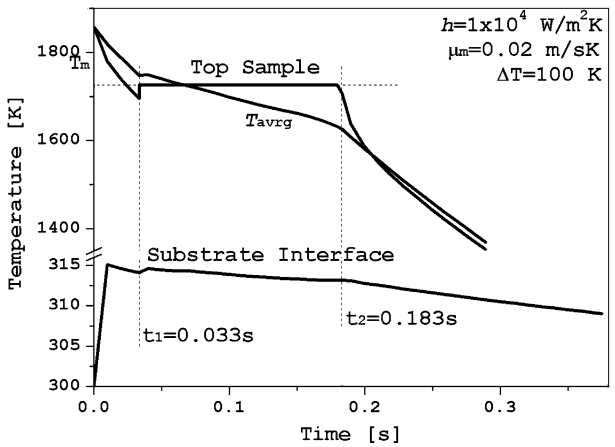

Fig. 7 Time-dependent temperature profiles for the sample (top surface temperature and the average temperature, T_{avrg}) and the substrate interface surface during solidification of nickel on copper substrate (with undercooling)

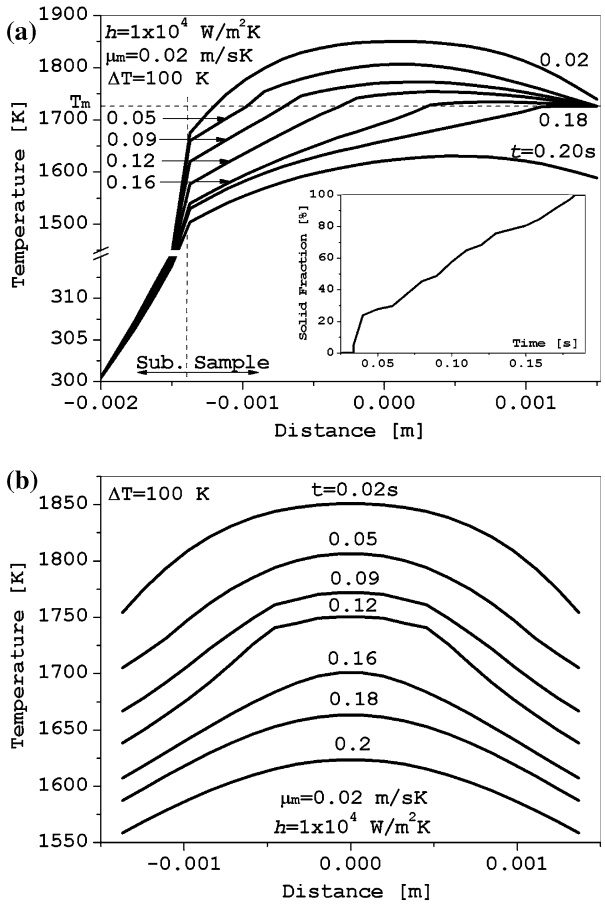

Fig. 8 Temperature evolution across the sample center during solidification of nickel on copper substrate (with undercooling) in (**a**) vertical (substrate–sample) and (**b**) horizontal directions. The inset gives corresponding time-dependent solid fraction

0.033 s, developed the concave solidification front with rather thick lateral solidified layers. The sample middle is now at lower temperature but still liquid. This process continues up to 0.12 s. Then the sample middle solidified and for 0.16 s almost 80% of the sample is solidified, whereas at 0.18 s melt exist only around the sample top surface. Using computed temperature profiles (Fig. 8b) the cooling rate of the sample center during solidification can be estimated to be on the order 1×10^3 K/s. This value agrees with typical cooling rates of the spherical arc-melted specimens that were estimated to be higher than 10^3 K/s [12]. Full solidification of the sample takes place at 0.183 s and single phase cooling down continues.

Although the undercooling determines kinetics of solidification, the heat transfer through the substrate defined by the heat transfer coefficient is also important parameter. Figure 9 shows two temperature profiles (for $h = 3 \times 10^4$ W/m^2 K and $h = 5 \times 10^4$ W/m^2 K) for the sample (at its top and the average temperature) and the substrate. Increasing h at constant μ_m enhances the rate of internal heat extraction through the substrate producing shorter solidification time (from $t_2 = 0.16$ s to $t_2 = 0.13$ s) and shorter cooling time (higher cooling rate) after solidification.

Conclusion

In this paper we have proposed computer-based method for simulation of rapid solidification of spherical sample on colder substrate as heat sink. Introduction of CVs for definition of the sample domain allowed us to track curved interface solid–liquid across neighboring CVs of different phases in both horizontal and vertical directions. Assuming that the interface configuration sample–substrate is stable during the entire solidification process, we have defined 2-D finite difference heat conduction model with moving solid–liquid interface for solidification with and without undercooling. The method is semi-implicit with the explicit schemes during single phase cooling (melt cooling and solidified sample cooling) and with fully implicit schemes for rapid solidification (two phase). The model developed includes the effects of the heat transfer through the substrate, but also through the sample surface by the convection and the radiation. Although the mathematical formulation and the solution methodology developed are general, pure nickel spherical sample on copper substrate is used as model experiment in order to illustrate the validity of the method. Computed thermal histories for both solidifications without and with undercooling showed that this technique is able to study quantitatively the whole solidification process, including the recalescence in the case of undercooled melt. We believe that with some modification this method can also be used, as predictive

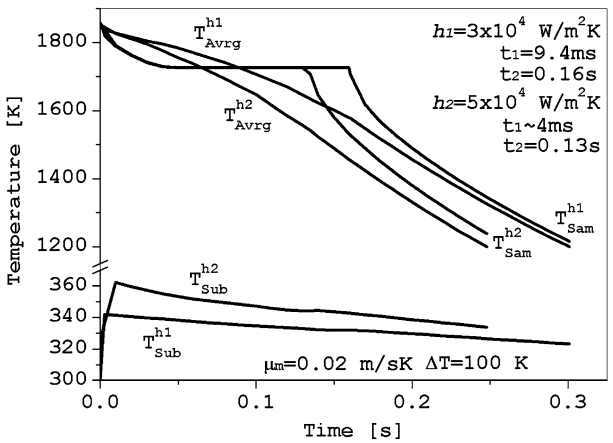

Fig. 9 Dependence of the sample top surface temperature (T_{Sam}), the average temperature (T_{Avrg}) and the substrate interface surface temperature (T_{Sub}) on the interfacial heat transfer coefficient during solidification of nickel on copper substrate (with undercooling)

method for control of rapidly solidifying sample for achieving desired sample microstructures and properties.

Acknowledgements The first author would like to thank the Japan Society for the Promotion of Science (Invitation Fellowship No. L-06544).

References

1. Anantharaman TR, Suryanarayana C (1971) J Mater Sci 6:1111
2. Sundarraj S, Voller VR (1993) Int J Heat Mass Transfer 36:713
3. Wang G-X, Matthys EF (1992) Int J Heat Mass Transfer 35:141
4. Kim C-J, Kaviany M (1992) Int J Heat Mass Transfer 35:1143
5. Zhang H, Prasas V, Moallemi MK (1996) Numer Heat Transfer B 29:399
6. Wang G-X, Matthys EF (1993) Heat and mass transfer in materials processing and manufacturing, HTD-261, pp 35–44
7. Nikolic ZS, Yoshimura M, Araki S (2005) Mater Sci Forum 494:381
8. Minkowycz WJ, Sparrow EM, Schneider GE, Pletcher RH (eds) (1988) Handbook of numerical heat transfer. Wiley, New York, p 68
9. Incropera FP, DeWitt DP (2002) Introduction to heat transfer. John Wiley & Sons, New York
10. Levi CG, Mehrabian R (1982) Metall Trans A 13A:221
11. Nikolic ZS, Yoshimura M (2006) The 3rd international symposium on advanced ceramics (ISAC-3), Innovation of Ceramic Science and Engineering, December 11–15, 2006, Singapore (Session Advanced Processing of Ceramics: Sintering, No: I12-A10), p 367
12. Yamada T, Yoshimura M, Somiya S (1986) High Temp – High Press 18:377